

In-vivo Tongue Stiffness Measured By Aspiration: Resting vs General Anesthesia.

K.D.R. Kappert^{1,2*}, MSc
N. Connesson*, PhD³
S.A. Elahi, PhD³
S. Boonstra^{1,2}, MSc
A.J.M. Balm, MD, PhD^{1,4}
F. van der Heijden, PhD^{1,2}
Y. Payan, PhD³

- ¹ Head & Neck Oncology and Surgery, Netherlands Cancer Institute, Amsterdam, The Netherlands;
² Robotics and Mechatronics, Technical Medical Centre, University of Twente, Enschede, The Netherlands;
³ TIMC-IMAG Laboratory, Grenoble Alpes University, Grenoble, France
⁴ Oral and Maxillofacial Surgery, Amsterdam UMC, University of Amsterdam, Amsterdam, The Netherlands.

Address for correspondence:

Kilian Kappert, MSc
The Netherlands Cancer Institute
Plesmanlaan 121
1066 CX Amsterdam
The Netherlands
Phone: +31205129731
E-mail 1: k.kappert@nki.nl
E-mail 2: k.d.r.kappert@utwente.nl (for open access)

Keywords

Tongue stiffness, General anesthesia, Tissue parameters, Aspiration device, Tongue cancer
*contributions of these authors are equivalent in the respective specialties.

Journal of Biomechanics, <https://doi.org/10.1016/j.jbiomech.2020.110147>.

Abstract

Tongue cancer treatment often results in impaired speech, swallowing, or mastication. Simulating the effect of treatments can help the patient and the treating physician to understand the effects and impact of the intervention. To simulate deformations of the tongue, identifying accurate mechanical properties of tissue is essential. However, not many succeeded in characterizing *in-vivo* tongue stiffness. Those who did, measured the tongue At Rest (AR), in which muscle tone subsides even if muscles are not willingly activated. We expected to find an absolute rest state in participants 'under General Anesthesia' (GA).

We elaborated on previous work by measuring the mechanical behavior of the *in-vivo* tongue under aspiration using an improved volume-based method. Using this technique, 5 to 7 measurements were performed on 10 participants both AR and under GA. The obtained Pressure-Shape curves were first analyzed using the initial slope and its variations. Hereafter, an inverse Finite Element Analysis (FEA) was applied to identify the mechanical parameters using the Yeoh, Gent, and Ogden hyperelastic models.

The measurements AR provided a mean Young's Modulus of 1638 Pa (min 1035 – max 2019) using the Yeoh constitutive model, which is in line with previous *ex-vivo* measurements. However, while hoping to find a rest state under GA, the tongue unexpectedly appeared to be approximately 2 to 2.5 times stiffer under GA than AR. Explanations for this were sought by examining drugs administered during GA, blood flow, perfusion, and upper airway reflexes, but neither of these explanations could be confirmed.

Introduction

Head and neck cancers are notorious for their negative impact on quality of life (Costa Bandeira *et al.*, 2008; Husaini *et al.*, 2014; Kreeft *et al.*, 2009; Lee *et al.*, 2014; Montero and Patel, 2015; van der Molen *et al.*, 2012). Treatment of tongue cancer, which accounts for approximately 20% of all head and neck carcinomas, can have a destructive effect on speech, swallowing, and mastication. The preferred treatment is surgery, but if the resulting post-operative functional loss is expected to be too disabling, organ-preserving chemoradiation and other alternatives can be considered (Sessions *et al.*, 2002; Shah and Gil, 2009). Due to the complex structures and systems involved in oral functions, a clinician cannot accurately predict the functional consequences of treatment. Effective patient counseling and treatment choice is, therefore, often an arduous task. Simulating the effect of treatments using biomechanical computer models can help the patient and the treating physician to understand the impact of interventions. In the past years, multiple biomechanical tongue models have been developed to simulate tongue function with and without simulated impairment caused by pathologies and/or treatment (Buchaillard *et al.*, 2007; Fujita *et al.*, 2007; Kappert *et al.*, 2019b; Van Alphen *et al.*, 2013; Vogt *et al.*, 2006).

To simulate realistic tissue behavior, choosing a proper constitutive model and identifying accurate mechanical properties is essential. Surgery or radiation can also induce fibrotic changes to tissue from which the extent may vary between patients and will affect the mechanical properties. Moreover, even for basic parameters such as the *in-vivo* stiffness values of the tongue in rest, no consensus has yet been reached. (Hermant *et al.*, 2017).

The human tongue mainly consists of muscles that behave as a nonlinear, time-dependent, inhomogeneous, and anisotropic material. Most of the constitutive model parameters in literature applied in human tongue tissue simulations are not based on real data because of the associated experimental difficulties (Buchaillard *et al.*, 2009; Gerard *et al.*, 2005; Pelteret and Reddy, 2012; Stavness *et al.*, 2012; Wang *et al.*, 2013; Wilhelms-Tricarico, 1995). According to Hermant *et al.* (2017), only three papers used experimental data to estimate the average tongue stiffness. Two of these experiments were performed *in-vivo* (Cheng *et al.*, 2011; Schiavone *et al.*, 2008) and one *ex-vivo* (Gerard *et al.*, 2005). *In-vivo* magnetic resonance elastography (MRE) was used by Cheng *et al.* (2011) in seven healthy participants, for which they found a mean Young's modulus of 7743 Pa. The MRE measurements provide higher stiffness values compared to what is expected for a tongue AR: first, due to the supine position of the individual, the tongue muscles are activated to keep an acceptable geometry. Second, the mechanical properties are measured using external 80 Hz vibrations transferred into the tongue tissue (Cheng *et al.*, 2011). The measured stiffness modulus may differ from the quasi-static elastic modulus due to the expected muscle frequency-dependent mechanical behavior (Clayton *et al.*, 2011).

Schiavone *et al.* (2008) measured tongue tissue properties *in-vivo* using a chamber with a circular aperture that was placed on the tongue and depressurized. The height of the tissue aspirated into the chamber was measured using a camera. Inverse identification of the tissue parameters was then performed using a Finite Element (FE) model of the aspiration experiment and Yeoh strain energy function.

With the same measurement system but activated muscles, the observed Young's Modulus was approximately 6 times higher (Schiavone *et al.*, 2008); muscle tongue activation thus impacts the observed stiffness. Furthermore, it should be noted that residual stresses and natural muscle tone persist even if muscles are not willingly activated (Fung, 1973).

Ex-vivo tissue is expected to have a higher Young's modulus because of the lack of vascularization and protein degradation (Gefen and Margulies, 2004; Kerdok *et al.*, 2006). However, the *ex-vivo* experiment of Gerard *et al.* (2005) (Table 5) showed a tongue Young's Modulus that was almost 2 times lower than the *in-vivo* experiment AR of Schiavone *et al.* (2008).

These phenomena raise the difficulty to define a reference muscle state, to perform an *in-vivo* measurement, and to set a simulation start point. From a practical point of view, this reference muscle state will always be a situation where internal stress and strain heterogeneities are present. It is the authors' opinion that such a reference muscle state should be defined with the lowest possible muscle activity, *i.e.* when only muscle tone remains. We expect to find this 'absolute' rest state in participants under General Anesthesia (GA).

Using an improved version of the aspiration method, initially presented in Elahi *et al.* (2019, 2018), the tongue mechanical properties will be measured (1) 'at rest' (AR) and (2) under GA, on 10 individuals without any history of tongue disease. As a first approximation, the tongue tissue will be considered as a homogeneous uniform isotropic material. The used inverse identification method and the impact of different constitutive models will be discussed. The main goals of this study are to estimate the following for the human tongue:

- The measurement reproducibility in each participant and variability between participants.
- The differences in apparent behavior of tissue between AR and under GA.
- The tissue parameters of the tongue for simulation purposes.

Method

Measurement setup

Elahi *et al.* (2018) proposed a modified version of the aspiration device of Schiavone *et al.* (2008) (Figure 1A). Any camera was removed from the system to diminish design constraints; the measurement of the tissue height was replaced by a volume measurement using a medical pump. The system and method used in this paper are comparable to the one used in Elahi *et al.* (2019) where more details are reported. It provided results with a maximum error of +8.8% compared to classical tests such as tensile or bulge tests. In this work, a custom suction cup (Figure 1B and C) was printed in 3D with a Form 2 printer (Formlabs, Somerville USA) using dental SG (biocompatible resin). The suction cup has an inner diameter of 10 mm and a wall thickness of 0.5 mm. (Figure 1B).

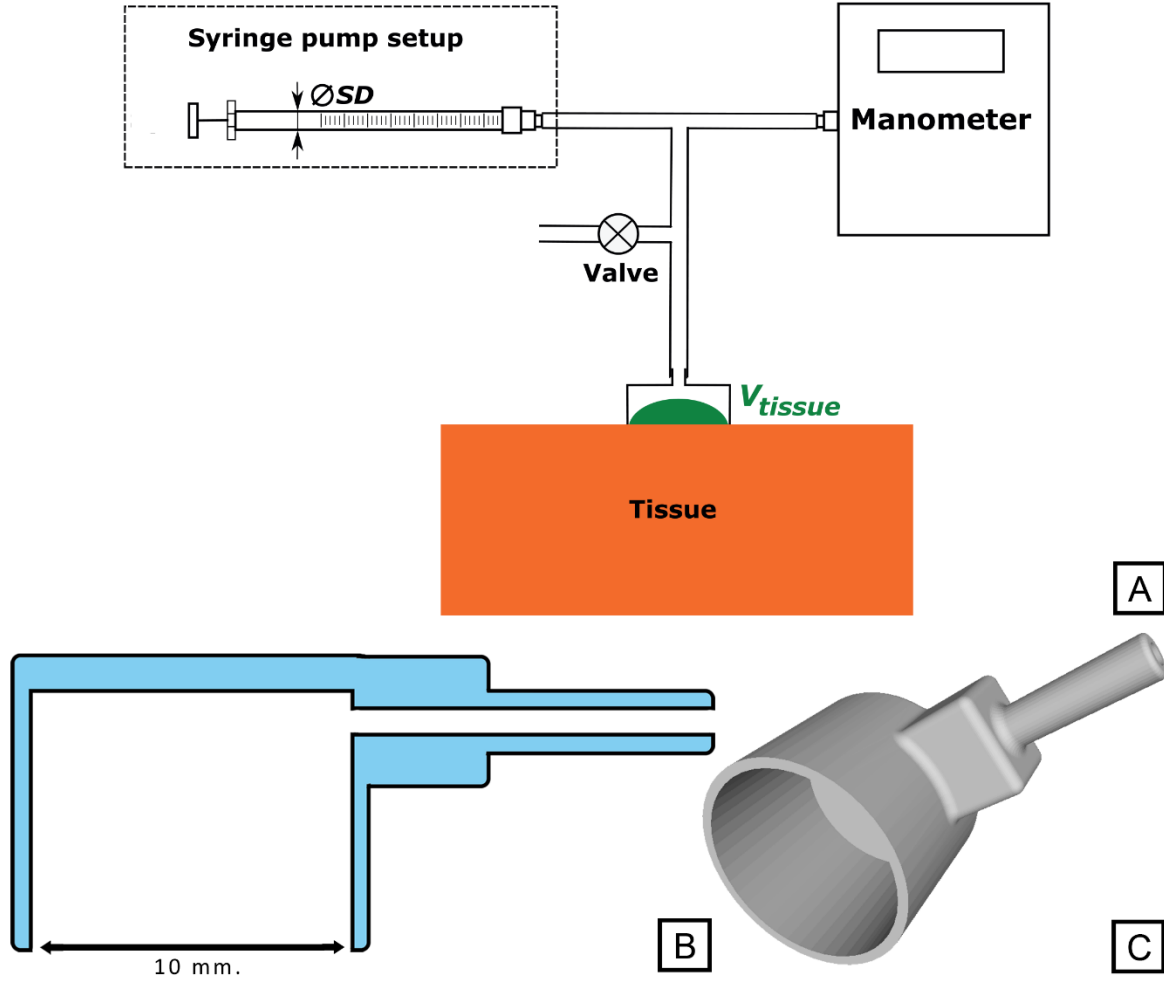


Figure 1: A schematic drawing of the volume-based aspiration setup (A) Adapted from Elahi et al. (2019), the suction cup cross-section with an aperture diameter of 10 mm, a wall thickness of 0.5 mm, and side tube (B), and a 3D render of the cup (C).

A programmable syringe pump (pump 11 elite, Harvard Apparatus, Holliston USA) was used to remove an air volume V^{total} from the system at a fixed rate of $0.6 \text{ mL} \cdot \text{min}^{-1}$. The syringe pump in combination with a 3 mL syringe provided a precision of $\pm 0.002 \text{ ml}$ (Elahi et al., 2019). The corresponding pressure P was measured using a manometer (DP205, MECOTEC GmbH, Hattingen, Germany) with a precision of 0.004 mbar.

The measured total volume curve $V^{total}(P)$ retrieved from the system consisted of both the tissue aspirated inside the suction cup and changes in the intrinsic system volume (air expansion and stiffness of components). The changes in system volume V_{system} were assessed by testing a non-deformable material (self calibration) whereby only the response of the system $V_{system}(P)$ is measured. The aspirated tissue volume at each pressure was then estimated using the following relation:

$$V_{tissue}(P) = V^{total}(P) - V_{system}(P) \quad 1$$

The tissue volume $V_{tissue}(P)$ was normalized into an adimensional and scale-independent Shape parameter S using a half sphere volume as reference (Figure 1A). A typical Pressure-Shape curve obtained

on human tongue tissue is plotted in Figure 2. Such a curve contains information about the mechanical properties of the tongue tissue.

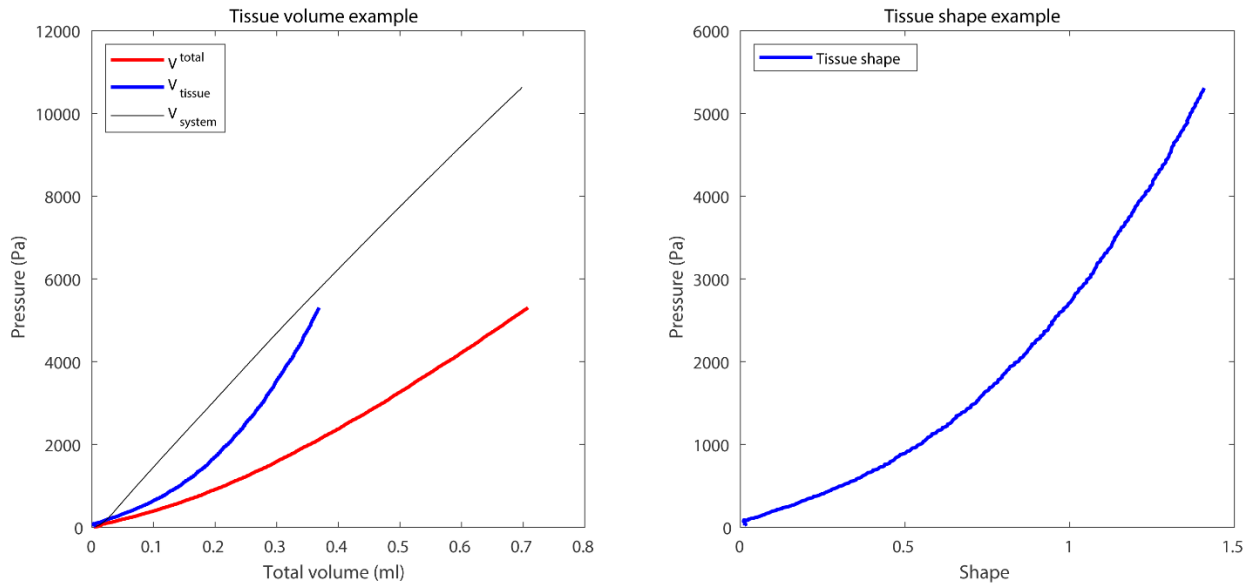


Figure 2: The left graph shows the raw experimental data and associated tissue volume $V_{tissue}(P)$ and the right graph shows the normalized curve.

Measurement protocol

The measurements AR and under GA were performed using as identical protocols as possible. Ten participants scheduled for surgery without any history of tongue disease were selected from the gynecology and urology department of the Netherlands Cancer Institute. Since this was the first study of its kind, sample size calculation was not applicable.

The measurements AR were performed on seated participants a week before or a month after surgery. Measurements under GA started one hour after the beginning of surgery. All participants had an epidural catheter and were infused according to the same anesthesiologic protocol with solutions of Propofol, Sufentanil, Remifentanyl, Efidrine, and Rucurionium using different dosages.

A sterilized suction cup was placed on the dorsum of the tongue, away from the midline (Figure 3). A minimum of five measurements was performed successively, each time removing the cup for 30 seconds between each measurement so that the tissue had time to restore to its initial state. When possible, the measurement location was alternated (Figure 3A, yellow areas) to avoid waiting time.

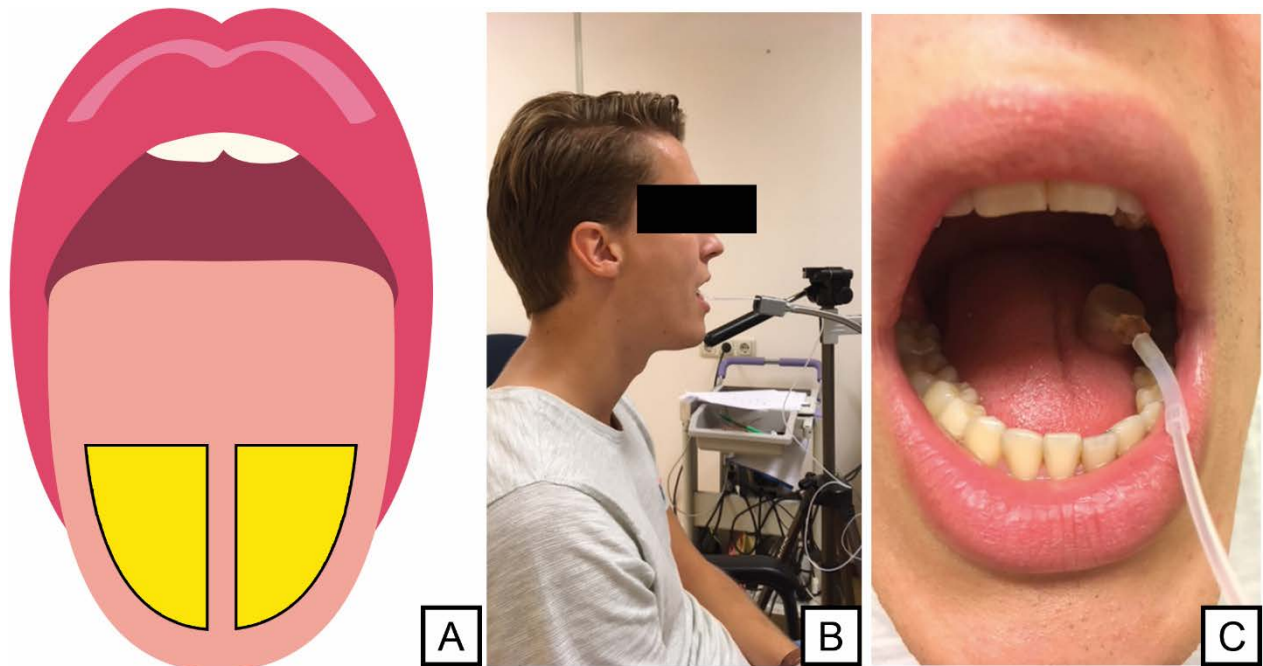


Figure 3 An Illustration of the human tongue (A) and the applied suction cup on the tongue of a participant (B, C). During the measurements, a sterilized cup is placed on the yellow area on the tongue's surface. (Background image designed by Freepik)

Pump start and pressure measurement were synchronized using custom software. Moisture (water and saliva) and small initial pre-load, applied by placing the cup by hand, helped to prevent leakage at the measurement start (no secondary syringe as in Elahi *et al.* (2019) so as not to affect the air quantity in the system tubes). The pressure change due to this pre-load was monitored and subsequently removed from the experimental data. Any initial leakage could be detected during this stage; erroneous measurements were immediately discarded.

Measurements were stopped at a pressure threshold of -55 mbar to avoid discomfort. All procedures performed involving human participants were in accordance with the ethical standards of the medical ethical committee of the Netherlands Cancer Institute (ref: N18EMT) and with the 1964 Helsinki declaration and its later amendment. Informed consent was obtained from all individual participants.

Tissue properties analyze and parameter identification

The main features of the experimental Pressure-Shape curves $S_{exp}(P)$ (Figure 2) are its initial slope and variation with pressure. These two features are impacted by the material properties (apparent Stiffness, Incompressibility, strain-stiffening relation) but also by phenomena such as the residual load applied to the cup, the cup-tissue friction coefficient, the tongue size compared to aperture diameter, the boundary conditions, the experimental reproducibly difficulties due to system temperature change and the cup positioning.

Inverse parameters identifications are inherently impacted by these hypotheses and the constitutive model choice. To circumvent these difficulties during the first analysis step, the Pressure-Shape experimental curves slope A_{RS} were evaluated at a Reference Shape R_S ($R_S=0.1$ and 0.5):

$$A_{RS} = \left. \frac{dP}{dS_{exp}} \right|_{S_{exp}=R_S} \quad 2$$

The Pressure-Shape stiffening was characterized by the ratio B_{Stiff} :

$$B_{Stiff} = \frac{A_{0.5}}{A_{0.1}} \quad 3$$

In this study, stiffness A_{RS} and stiffening ratio B_{Stiff} were compared both for AR and under GA.

In a second step, the Young's Modulus range was extracted from the experimental data. An inverse analysis was performed by simulating the measurement Pressure-Shape $S_{FE}(P)$ using a Finite Element (FE) model (Figure 4a) in 2D assuming an axisymmetric axis in a FE software (ANSYS). The aperture was clamped and a friction coefficient of $\mu = 0.2$ was chosen for the contact between tissue and aperture. Negative pressure was applied on the surface inside the aperture; the outer tissue boundaries remained free. This method was successfully validated on a silicone phantom (Elahi *et al.* (2018), Elahi *et al.*, 2019).

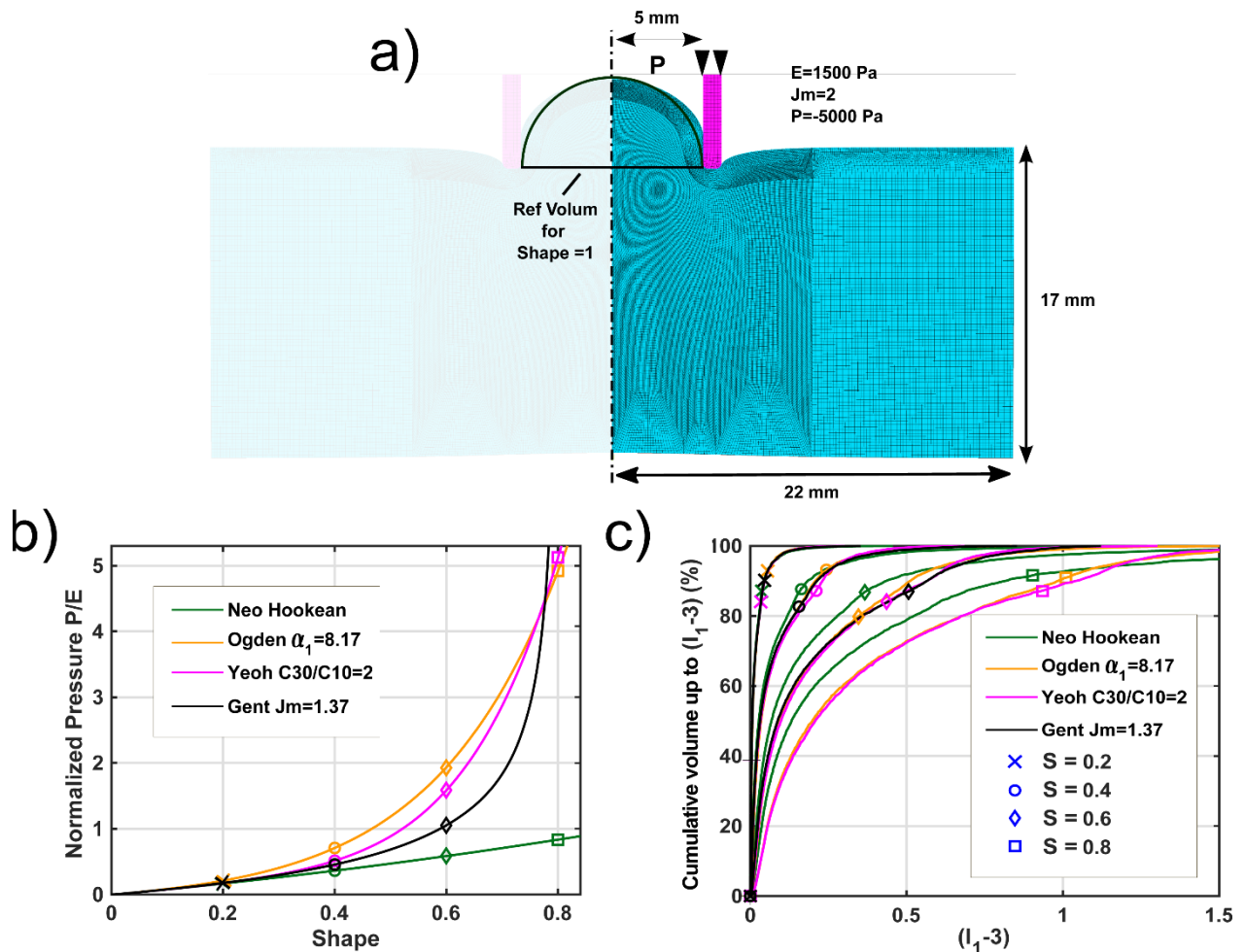


Figure 4: a) Simulated FE, Boundary conditions, meshing (36000 Q8 axisymmetric elements), and an example of the deformed shape $S=1$. b) Normalized Pressure-Shape curve for different material models and chosen parameters representative of the experimental results. c) Illustration of cumulated volumic

repartition in the tissue under the aperture (Depth=Radius=0.75 Diameter) for which local invariant is lower than an $(I_1 - 3)$ threshold. Specific points presented in figure b) for shapes 0.2, 0.4, 0.6 and 0.8.

The minimized function was defined in the least mean square sens to optimize both shape and slope fitting:

$$\begin{aligned} \Phi &= \beta \quad \Phi_1 \quad + (1 - \beta) \quad \Phi_2 \\ &= \beta \quad \underbrace{\sum_{i=1}^I \epsilon_i^2}_{\text{Shape fitting quality}} \quad + (1 - \beta) \quad \underbrace{\sum_{k=1}^K \left(\frac{d\epsilon}{ds}\right)_k^2}_{\text{Slope fitting quality}} \end{aligned} \quad 4$$

where

- ϵ_i is the shape fitting error for a measurement at pressure P_i ($\epsilon_i = (S_{exp} + V_o - S_{FE})_i$) and V_o is the value for an unknown volume due to the plastic-rubber backlash of the syringe piston occurring at the measurement start.
- $\left(\frac{d\epsilon}{ds}\right)_k$ is the derivative of the fitting error ϵ regarding the shape, evaluated at the pressure P_k . Function Φ_2 thus represents the slope fitting error at the start of the curve.
- I is the number of experimental points, K is a chosen number of points so that $K = \text{round}(I/5)$ to reduce the slope fitting error at the start of the curve.
- β is a value in the range $[0 \ 1]$ to focus the fitting on either the slope at measurement start or the global curve.

Different material model formulations (Table 1, Gent (Horgan, 2015), Yeoh (Yeoh, 1993), and Ogden (Ogden, 1984)) have been used in their fully incompressible formulation (Poisson ratio $\nu=0.5$) to describe the tongue tissue behavior under aspiration (Table 1).

Table 1: Overview of different constitutive models on biological tissue and their strain energy density functions found in the literature. The equivalent Young's modulus assumes a Poisson coefficient of 0.5.

Model	Strain energy density function		Equivalent Young's modulus	Application illustration
Gent	$W = -\frac{\mu J_m}{2} \ln\left(1 - \frac{I_1 - 3}{J_m}\right)$	with μ the shear modulus. J_m is the stiffening parameter and its' maximum value is of $(I_1 - 3)$. $I_1 = \lambda_1^2 + \lambda_2^2 + \lambda_3^2$, where $(\lambda_i)_{i=1,3}$ are the principal stretches	$E = 3\mu$	(Elahi <i>et al.</i> , 2019, 2018; Rashid <i>et al.</i> , 2012)
Ogden	$W = \frac{\mu_1}{\alpha_1} (\lambda_1^{\alpha_1} + \lambda_2^{\alpha_1} + \lambda_3^{\alpha_1} - 3)$	where $\mu_1 \alpha_1 > 0$. with α_1 the stiffening parameter.	$E = \frac{3\alpha_1 \mu_1}{2}$	(Budday <i>et al.</i> , 2017; Rashid <i>et al.</i> , 2012)
Yeoh _{C2} oc30	$W = C_{10}(I_1 - 3) + C_{20}(I_1 - 3)^2 + C_{30}(I_1 - 3)^3$	with I_1 the first invariant of the Cauchy-Green strain tensor. C_{20} and C_{30} are the stiffening parameters.	$E = 6C_{10}$	(Buchaillard <i>et al.</i> , 2009; Gerard <i>et al.</i> , 2005; Mehrabian and Samani, 2008; Sadeghnejad <i>et al.</i> , 2019; Schiavone <i>et al.</i> , 2010, 2009, 2008)
Yeoh _{C2} 0	$W = C_{10}(I_1 - 3) + C_{20}(I_1 - 3)^2$			
Yeoh _{C3} 0	$W = C_{10}(I_1 - 3) + C_{30}(I_1 - 3)^3$			

During the function \emptyset minimization, the FE Pressure-Shape curves were evaluated using pre-calculated FE databases. A model reduction based on the Principal Component Analysis method has been implemented (Lang *et al.*, 2009). A typical identification result is presented in Figure 5 using the data of patient 4 (AR). A single measurement and analysis take up less than one minute.

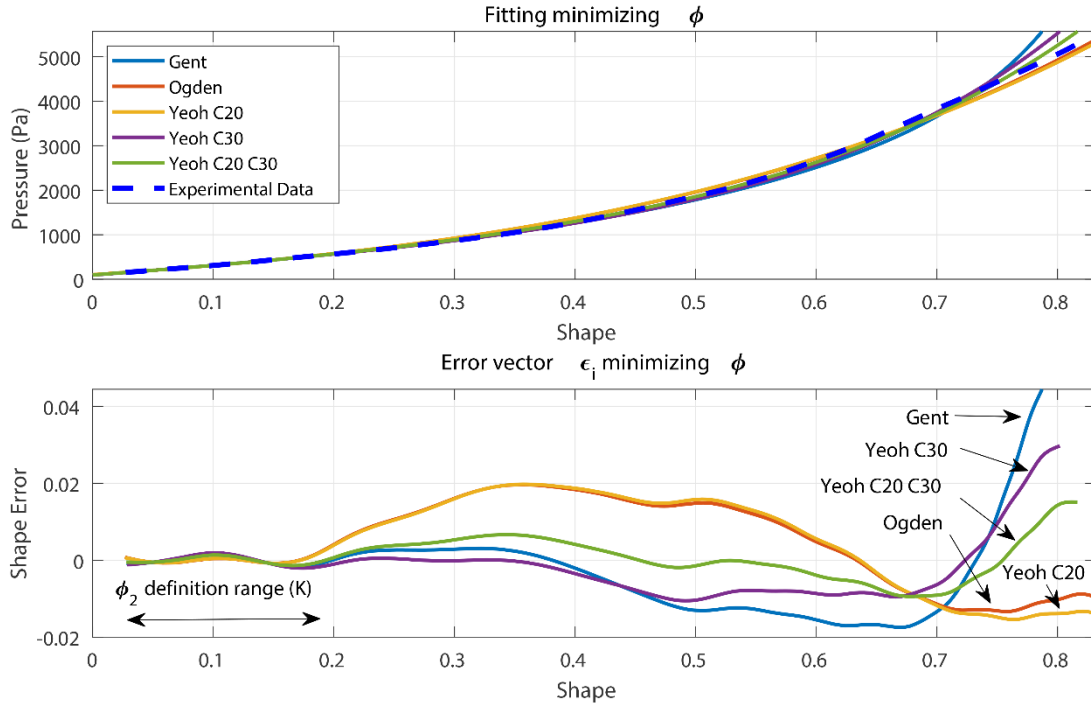


Figure 5: Fitting illustration (upper graph) and associated Shape error ϵ_i (lower graph) of the different models minimizing ϕ_2 in a measurement of participant #5.

Criteria must be defined to compare the models as they express different physical and stiffening behavior from the starting point of the Neo-Hookean model (Ogden, 1984). The model outputs have been compared studying (1) an equivalent Young's modulus (Table 1), (2) the Pressure-Shape curve fitting quality to the experimental curves (ϕ , ϕ_1 , ϕ_2 , Eq 4.), and (3) invariant strain fields ($I_1 - 3$) where I_1 is the first invariant of the Cauchy-Green strain tensor.

The strain invariant ($I_1 - 3$) fields, for each model and for specific shapes values, have been converted into cumulated volume repartition curves $f(I_1 - 3)$ (Figure 4c):

$$f(I_1 - 3) = \frac{V_{X < (I_1 - 3)}}{V_{\text{ref}}} \quad 5$$

where $V_{X < (I_1 - 3)}$ is the tissue volume for which the value is lower than the specific threshold ($I_1 - 3$). V_{ref} is the considered tissue volume around the aperture. All volumes have been evaluated in the un-deformed initial state.

Measurement variabilities

Additional measurements were performed to evaluate reproducibility ranges or potential biases in the measurements:

Bovine meat measurements: Seven measurements were performed *ex-vivo* on a piece of fresh bovine muscle at room temperature ($\sim 21^\circ$) using the same protocol. Such measurement will be considered as the gold standard situation for tissue passivity and environment reproducibility.

Temperature variations: While measurements were obtained under the same conditions at room temperature, exhaled air could have induced internal temperature (and thus pressure) changes in the

system AR, which was not present under GA due to the mechanical ventilator/intubation. The average effect of temperature variations was evaluated by immersing the suction cup in water with different controlled temperatures.

Friction and Poisson coefficients: The results are affected by friction and Poisson coefficients. Simulations were performed to numerically assess these parameters influence.

Statistical analysis:

For every 5 to 7 measurements per patient, the median and the Inter Quartile Range (IQR) are calculated.

To test if the measurements AR and under GA for patient *n* are from the same distribution (identical median and spread) the Mann-Whitney U test is used (Mann and Whitney, 1947). When $p < 0.05$, this hypothesis is rejected.

To test if the calculated medians AR and under GA over the whole population are from the same distribution, the Wilcoxon signed-rank test is used (Wilcoxon, 1947). When $p < 0.05$, this hypothesis is rejected.

The IQR is normalized by the median value to be converted in percentage to compare the variability between participants and situations:

$$Normalized\ IQR = \frac{IQR}{median} * 100\% \quad 6$$

Results

Half of the 10 participants were males and the mean age was 62 (Table 2).

Table 2: patient characteristics and number of included measurements per patient and per situation.

n	Gender	Age	Type of surgery	Department	Number of measurements AR/under GA
1	M	67	Pelvic Lymph Node Dissection	URO	5 / 6
2	W	62	Bladder resection	URO	5 / 7
3	W	63	Secondary Debulking Surgery	GYN	7 / 6
4	M	67	Nephrectomy	URO	5 / 6
5	W	59	Nephrectomy	URO	5 / 6
6	M	70	Pelvic Lymph Node Dissection	URO	6 / 6
7	W	49	Secondary Debulking Surgery	GYN	5 / 6
8	W	70	Pelvic Lymph Node Dissection	URO	6 / 7
9	M	55	Ureteral Surgery	URO	5 / 7
10	M	59	Nephrectomy	URO	6 / 6

The median and IQR of $A_{0.1}$ and B_{Stiff} were calculated and plotted as boxplots in Figure 6A and B. The *p* values of the Mann-Whitney U test are visible on the horizontal axis. Subsequently, the means of the Medians (μ_M) and the means of the IQR's (μ_{IQR}) for every patient AR and under GA are shown in Table 3 and Figure 6 for the A_{RS} and B_{Stiff} , respectively. The table also includes the results of the *ex-vivo* bovine meat measurement and the results of the Wilcoxon signed-rank test.

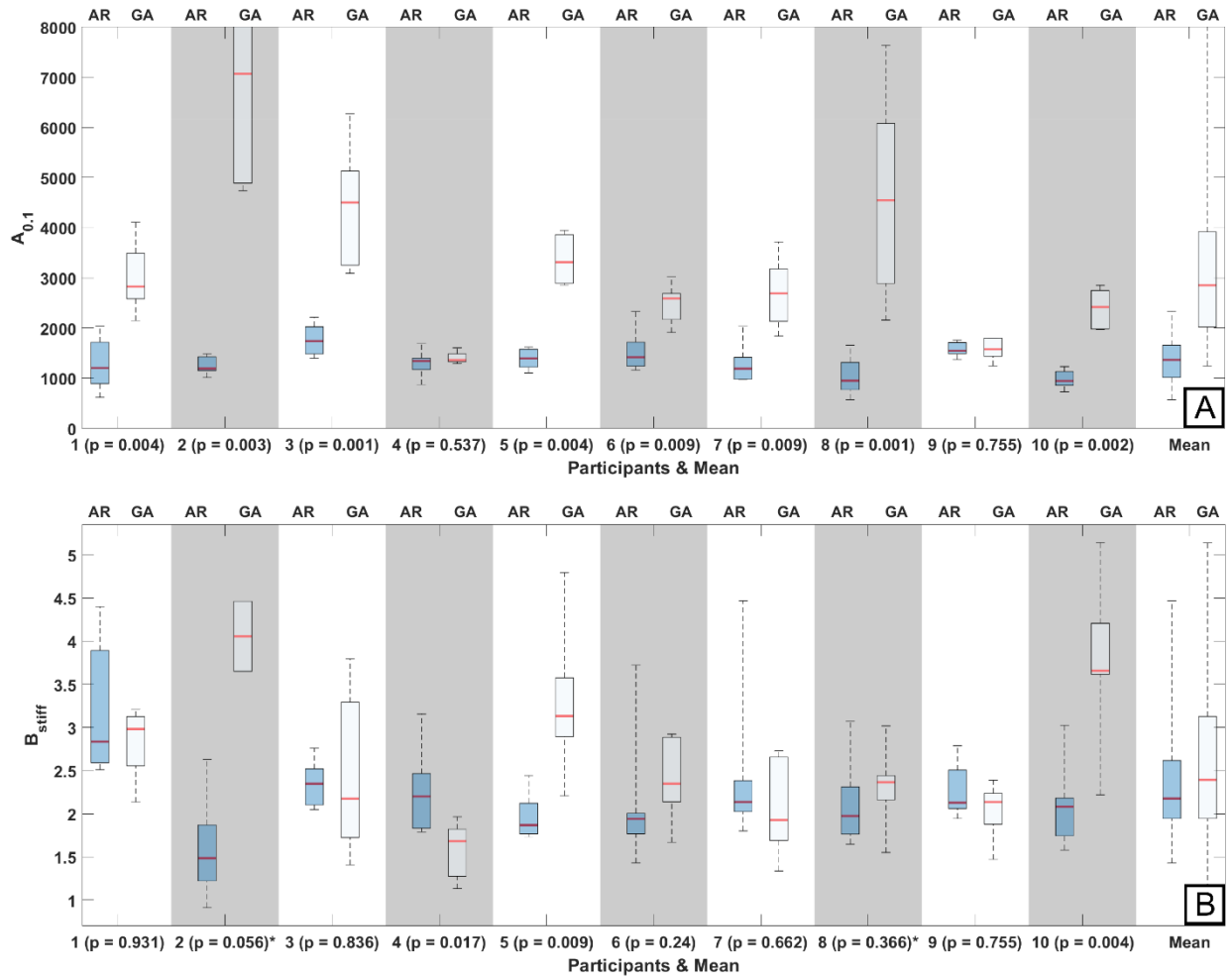


Figure 6: The dark blue boxplots show the median $A_{0.1}$ (A) or B_{stiff} parameter (B) and its IQR based on 5 to 7 measurements for every patient AR. The boxplots show the $A_{0.1}$ (A) or B_{stiff} parameter (B) for participants under GA. On the abscise axis, the results of the Mann-Whitney U are shown for every patient.

Table 3: Stiffness parameter $A_{0.1}$ and stiffening parameter B_{stiff} of all patient combined and bovine measurements.

	Test	μM	Normalized μIQR
$A_{0.1}$	Bovine muscle (<i>ex-vivo</i>)	10185 Pa.S ⁻¹	13%
	At Rest	1292 Pa.S ⁻¹	18%
	under General Anesthesia	3289 Pa.S ⁻¹	63%
	Wilcoxon Signed-Rank (At Rest - under GA)	p = 0.002	
B_{Stiff}	Bovine muscle (<i>ex-vivo</i>)	1.20	15%
	At Rest	2.10	12%
	under General Anesthesia	2.65	37%
	Wilcoxon Signed-Rank (At Rest - under GA)	P = 0.19 (not sign)	

The initial Pressure-Shape slope $A_{0.1}$ is significantly higher (2.5 times) under GA than AR (Table 3, Figure 6A). The normalized μ IQR is 18% while AR, which is just above 13% obtained during the bovine *ex-vivo* measurement. Some of the measurements under GA show a lot of variation; the normalized μ IQR reaches 63%. Nevertheless, the Mann-Whitney U test confirms that in 8 out of 10 participants, the measurements are significantly higher under GA than AR (p -value lower than 0.05, Figure 6A).

Contrary to the $A_{0.1}$, the μ M of the stiffening factor B_{Stiff} is not significantly different in both situations (Table 3, Figure 6B).

Three and one measurement(s) were removed from participants 2 and 8, respectively; these measurements did not reach a shape value 0.5, preventing evaluation of the B_{Stiff} ratio value.

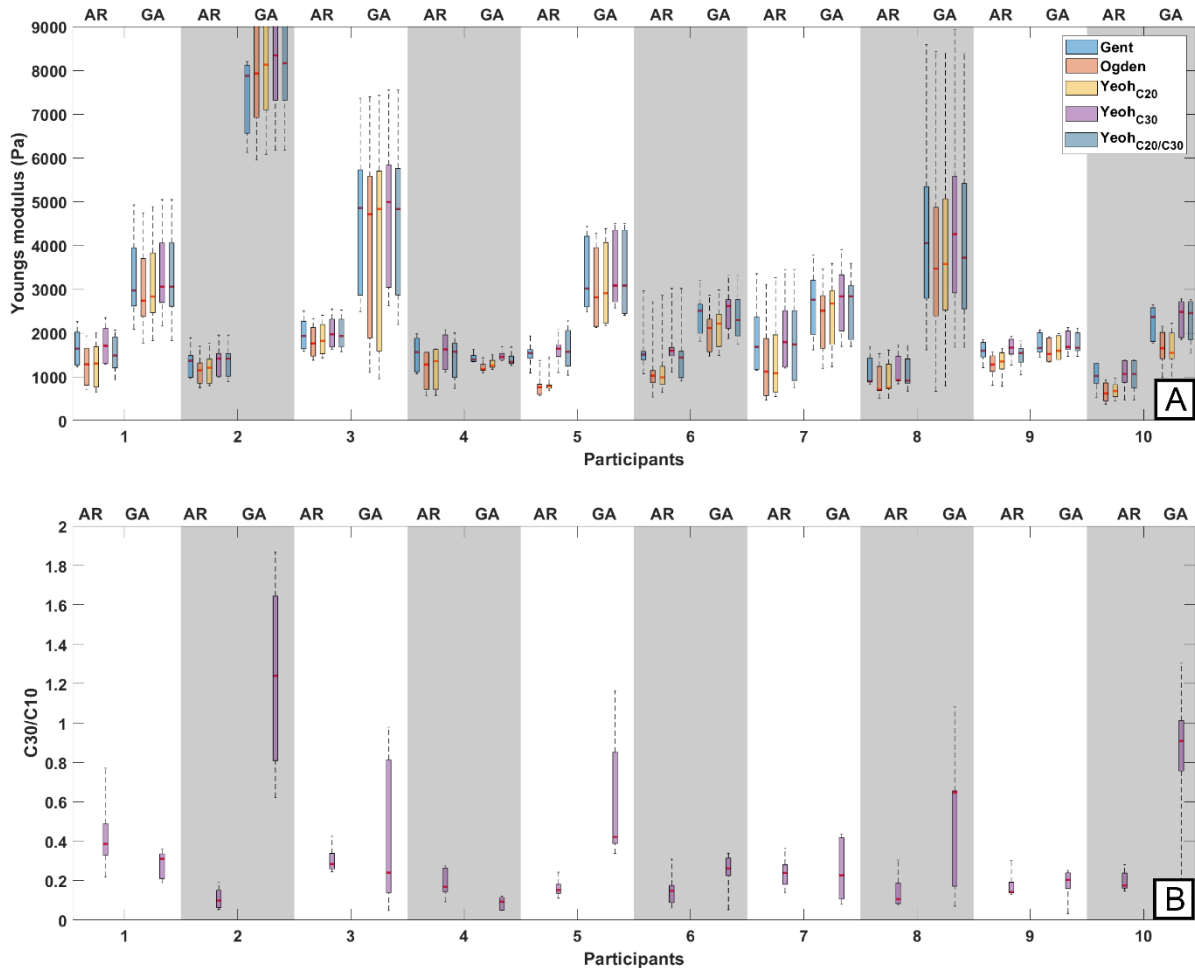


Figure 7: The colored boxplots show the median Young's modulus and IQR for the Gent, Ogden, Yeohc20, Yeohc30, Yeohc20/c30 for every participant AR and under GA (A). Only for the selected Yeohc30 model, the C30/C10 ratio is shown (B).

The identified Young's Moduli, for every patient and models from Table 1, are shown in Figure 7. Resemblance with $A_{0.1}$ from Figure 6 is striking: the median Young's Moduli differs from slope $A_{0.1}$ with a factor 0.88 (STD 0.11) to 1.14 (std 0.21) depending on the used constitutive model.

The global fitting quality for all the models is similar (ϕ_1 values lower than 0.052). The second part ϕ_2 of the ϕ function -criteria of proper fit at the start of the the Pressure-Shape slope- differs for each model.

Their average performances can be sorted as the following (best to worst median value): Yeoh_{c20/c30} (0.0003), Yeoh_{c30} (0.0007), Gent (0.0012), Yeoh_{c20} (0.0012), Ogden (0.0014).

In biomechanical modeling, two-parameter models are usually used in literature. The mean Youngs modulus by the Yeoh_{c30}, the best performing two-parameter model, is 1638 Pa AR and 3060 under GA. The parameter ratio C30/C10 (Figure 7B) provides a mean of 0.19 and 0.46 for all patients for AR and under GA, respectively.

Pressure-Shape curve and invariant repartition ($I_1 - 3$) for different material model have been computed for parameters chosen in a range representative of the experimental data (Figure 4b). The associated cumulated volume repartition curves $f(I_1 - 3)$ at specific shapes 0.2, 0.4, 0.6 and 0.8 (Figure 4c), have been computed using the volume V_{ref} as a cylinder with a height and a radius of 0.75 aperture diameter.

Measurement variabilities

Table 4: Parameter sensitivity analysis on the initial slope $A_{0.1}$ of Pressure-Shape curve. Parameters for the Yeohc30 material chosen to mimic real experimental data: C10=200 Pa ($E=1200$ Pa), C30=10Pa.

Performed test	Reference value X_0	Parameter tested range	Impact on Slope variation $\Delta A_{0.1}$ and std	Error percentage if slope $A_{0.1}$ of $1000 Pa \cdot S^{-1}$ (Yeoh C30, C10=200 Pa, C30= 10 Pa).
Average Temperature impact	25°C	Experimental test on calibration curve: [25°C – 37°C], 8 measurements each. Aperture temperature average stability in the mouth is reached in less than 60 seconds.	$30 \pm std 14.6 Pa \cdot S^{-1}$	$3 \pm std 1.5 \%$
Friction coefficient	0.2	Numerical tested range: [0.1 1]	$15.7 Pa \cdot S^{-1}$	1.6 %
Poisson ratio	0.5	Numerical tested range [0.499 0.5]	$5.6 Pa \cdot S^{-1}$	0.6 %

A parameter sensitivity analysis is presented in table 4. The impact on the initial Pressure-Shape curve slope $A_{0.1}$ is evaluated experimentally and numerically.

Discussion

To our knowledge, this is the first study that compared the tongue stiffness AR and under GA and the largest cohort of individuals that participated in tongue stiffness measurements at the moment of publishing.

Slope, stiffness and stiffening differences between AR and under GA

In this work, the initial slope $A_{0.1}$ and associated Young's Modulus of the tongue under GA are 2.5 and 1.9 times larger than AR, respectively. This difference is significant as shown in the Wilcoxon signed-rank test. On an individual level, the Mann-Whitney U test showed that the difference between AR and under GA is significant for 8 out of the 10 participants. The assumption that muscle tone is absent or lower under GA

is proven to be erroneous: results show an almost universal increase of tongue stiffness during anesthesia. Measurements AR thus provide a better reference state than under GA. These results are the opposite of what the authors expected and motivated extended experimental and numerical tests.

We found three plausible hypotheses in the literature to explain these results:

1. Sufentanil and Remifentanil, drugs administered during GA to all participants of this study, are reported to cause chest wall rigidity among other lipophilic opioids (Ackerman et al., 1990; Buxton et al., 2018; Dimitriou et al., 2014; Müller and Vogtmann, 2000). The frequently administered Rocuronium, a neuromuscular blocking agent, could counteract these effects by causing paralysis of skeletal muscle. However, few studies can be found about the interaction of the combined pharmaceuticals during anesthesia for muscle activation, and for the tongue in particular (Nakada et al., 2009). Analysis of the administered pharmaceuticals could not fully explain the exceptions of the two participants (4 and 9) who showed an identical stiffness under GA and AR.
2. Upper airway reflexes, activated by intubation under GA, are not always completely suppressed during general anesthesia (Tagaito et al., 1998). Such (remnants of) reflexes are unequally pronounced among humans and depend on the depth of anesthesia, which could explain the observed patient-specific singular absence of stiffening in participant 4 and 9 (Davies et al., 1995) but could not be confirmed.
3. The lack of movements and administered drugs under GA alter blood flow and perfusion. It could in turn affect the identified rigidity (Akata, 2007; Schwarte et al., 2008). Manually palpating tongue tissue under GA and AR, unfortunately, did not provide a subjective correlated observation as measurements took place days apart. The tongue under GA also showed a more persisting tissue deformation after aspiration. The tissue deformation was resolved quicker by palpating the tongue.

The stiffening ratio B_{stiff} shows that the slope was more than doubled from shape 0.1 to 0.5 (Figure 6B, Eq. 3). This effect is translated into a C30/C10 ratio for the Yeoh C30 model (Figure 7B): the median C30/C10 ratio value is in the range of [0.1 - 0.5] for 70% of participants both under GA and AR. This ratio range can be implemented in numerical models when assuming a perfectly incompressible material.

Measurement uncertainties

Given the unexpected results for the observed experimental difference between AR and under GA, the measurement method has been challenged with different phenomena using the initial slope $A_{0.1}$ as criteria (Table 4).

Variability of experimental slope $A_{0.1}$

The reproducibility of the method on biological tissues has been experimentally evaluated during the bovine meat *ex-vivo* test, assuming stable material parameters and a comparable situation with *in-vivo* testing (tissue compressibility, friction coefficient, load, temperature, etc): the normalized μ IQR of *ex-vivo* bovine meat is 13% of the median initial slope $A_{0.1}$. The reproducibility limitations of the method itself can thus not account for normalized μ IQR of 18% and 63% for the patient measurements (Table 3). The variability during the measurements AR could be caused by small uncontrolled tongue movements or breathing. During GA, the often cumbersome accessibility of the tongue made replacing the suction cup at the same place difficult and, therefore, less reproducible. Also, phenomena explained in the previous section could induce a change in material stiffness between or during measurements.

An average temperature difference in the mouth between AR and under GA is expected due to breathing/intubation. During the immersion tests, an average temperature difference as high as 12°C

surrounding the cup (37°C or 25°C room temperature water) proved to have a negligible effect on the initial slope $A_{0.1}$ ($3 \pm \text{std} 1.5\%$, Table 4).

A residual load, exercised by the weight of the suction cup and the tube, was present at both the measurements AR and under GA. The normal load contribution of the cup to the surface induced by the tube has been measured with a precision balance and was found to be lower than one gram, which is considered negligible in respect to other devices used in literature (Nava et al., 2008; Schiavone et al., 2008), or commercial products such as the Cutometer (Courage and Khazaka, Köln, Germany).

Parameter influencing the extracted Young's Modulus

The aspiration process has been validated on non-stiffening silicon objects in Elahi *et al.* (2019, 2018). It provided results with a maximum error of +8.8% compared to classical tests such as tensile or bulge tests. The adjustments made in the method provided similar results and identification range (experimentally checked, not presented).

Identifying parameters for an *in-vivo* stiffening material yet presents more challenges: the Ogden, Gent, and Yeoh model formulations (Table 1) are only able to approximate the real material stiffening behavior (model misspecification). This leads to drastically different equivalent Young's moduli if only the shape distance is minimized ($\emptyset = \emptyset_1$, $\beta = 0$, Eq. 4), even for satisfying global fitting results (results not presented). A value $\beta \in [0.1 \ 0.9]$ however provides an almost model-independent Young's Moduli (Figure 7A, $\beta = 0.5$) for satisfying fitting. The independency of the Identified Young's Modulus to the model formulation was considered a validation of the inverse method and chosen minimized function.

Initial slope $A_{0.1}$ is properly fitted thanks to the part \emptyset_2 of the minimized function \emptyset (Eq. 4). Obtaining a Young's Modulus almost proportional to the initial slope $A_{0.1}$ is thus an expected result.

Poisson and friction coefficient effects on the Pressure-Shape curve initial slope $A_{0.1}$ are below 1.6% for the tested ranges and are considered negligible compared to experimental reproducibility.

Young's modulus identification & literature comparison

The Yeoh_{c30} was the best performing two-parameter model in this study and is therefore compared to other literature. The median Young's modulus from all participants is 1638 Pa (min 1035 – max 2019) for AR and 3060 Pa (min 1477 – max 8930) for under GA.

The identified Young's modulus AR is 2.4 times smaller than the AR measurement of Schiavone *et al.* (2008) with a Yeoh_{c30} model and 30% smaller than the *ex-vivo* cadaver measurement of Gerard *et al.* (2005) with a Yeoh_{c20} model (Table 5). Both the Young's modulus AR and under GA are more than 2 times smaller than *in-vivo* MRE (Cheng *et al.*, 2011) and 8 to 16 times smaller than the "activated" tongue measurement of Schiavone *et al.* (2008). Aside from Cheng *et al.* (2011), all results of the cited *in-vivo* studies were obtained only from one participant.

Table 5: Comparison of measured Young’s modulus (Yeohc30) with other literature.* Equivalent tongue Young’s modulus (Pa) at small strain, **mean of 2 measurements.

Reference	(median) Young’s Modulus* of tongue E (Pa) and range	Ratio E Literature value / E _{AR}	Case	Muscle activity	Method	Material model	Participants
This paper	1638 (1035 – 2019)	N.A.	<i>In-vivo</i>	‘AR’	Aspiration (VLASTIC)	Yeoh _{c30}	10
This paper	3060 (1477 – 8930)	1.9	<i>In-vivo</i>	‘under GA’	Aspiration (VLASTIC)	Yeoh _{c30}	10
Gerard <i>et al.</i> (2005)	1140 (NA)	0.7	<i>Ex-vivo</i>	“none”	Indentation	Yeoh _{c20}	1
Schiavone <i>et al.</i> (2008)	3939 (3690 – 4188)**	2.4	<i>In-vivo</i>	‘AR’	Aspiration (LASTIC)	Yeoh _{c30}	1
Schiavone <i>et al.</i> (2008)	26634 (NA)	16.3	<i>In-vivo</i>	“Activated”	Aspiration (LASTIC)	Yeoh _{c30}	1
Cheng <i>et al.</i> (2011)	8100 (6630 – 9270)	4.9	<i>In-vivo</i>	“tongue against the palate”	MRE	Viscoelastic model	8

Young’s Moduli measured *in-vivo* (Table 5), injected into biomechanical models, usually prove too stiff to simulate realistic tissue deformations (Buchillard et al., 2009, 2007; Kappert et al., 2019b). This is substantiated by Hermant *et al.* (2017) who simulated the tongue movements in the direction of the pharyngeal wall using both a common tissue stiffness for tongue models ($E = 6222$ Pa) and a lower stiffness ($E = 1116$ Pa) based on the *ex-vivo* experiments from Gerard *et al.* (2005). They found much more realistic behavior using the lower stiffness. The identified Young’s Modulus range obtained of the ten measured participants in this work corroborates these results.

Limitations and Perspectives

To the authors’ knowledge, no artificial material presents a mechanical behavior close to that of the tongue (Young’s modulus and stiffening). This prevents the definition of a real gold standard to perform a fair comparison of identified Young’s Modulus for the whole method using aspiration or classical testing. The present method could only be validated on artificial non-stiffening material (Elahi *et al.* (2019, 2018)). However, the identification of a similar Young’s modulus on different material models makes the method trustworthy.

Numerical Pressure-Shape curves are almost independent (for the simulated parameters) of the model for a Shape upto 0.2 (Figure 4b), associated with $(I_1 - 3)$ values over the tissue volume in a range of [0 0.5] (Figure 4c). During a uniaxial tensile test, $(I_1 - 3) = 0.5$ correspond to a principal stretch of 1.46. The predicted $(I_1 - 3)$ volumetric repartition differs between models for shapes greater than 0.4 (Figure 4c): local stiffening induces strain locking; the deformation is spread differently to less stressed material parts. No experimental field data are provided in this study to select the most relevant model according to this criteria. Moreover, the obtained Pressure-Shape curves do not provide insight into all the tongue tissue properties (nonlinear, time-dependent, inhomogeneous, and anisotropic material).

As many factors influence the tongue stiffness under GA, a more controlled protocol is required to explain why tissue is stiffer under GA than AR. The three plausible hypotheses mentioned in the discussion could be tested (EMG measurements to evaluate muscle activity and gag reflex during anesthesia, administration of single drug as Rocuronium, propofol, fentanyl, *etc.*). Identifying the factors that lead to these surprising results could give insight on how to define a better reference state for the tongue. However, the clinical significance would be small for such an invasive study to be performed on humans.

Conclusion

The stiffness of the tongue in 10 participants was measured AR and while under GA during surgery. While aiming to measure the stiffness of the tongue without muscle tone, the tongue unexpectedly appeared to be approximately 2 to 2.5 times stiffer under GA. While several hypotheses can potentially explain this behavior, no definitive answer could be provided with the current data. Between patients, the measurements AR were comparable and proved to be as reproducible as *ex-vivo* measurements using the same method. However, this did not apply to the measurements under GA. Identification using a two-parameter Yeoh constitutive model showed that the Young's modulus of the tongue in the relaxed condition AR is approximately 1638 Pa and the C30/C10 ratio 0.19.

Acknowledgments

With special thanks to Kicky van Leeuwen and Maarten van Alphen for assisting during the measurements and to the nurse practitioners of the urology and gynecology for assisting with the inclusion of participants.

This study was financially supported by private funding from the Virtutis Opis Foundation (www.anbiportal.nl/web/svo), Mr. B. Verwelius† and, Mr. W. de Graaf. The Department of Head and Neck Oncology and Surgery of the Netherlands Cancer Institute received a research grant from Atos Medical AB (Malmö, Sweden, www.atosmedical.nl). The funders had no role in study design, data collection and analysis, decision to publish, or preparation of the manuscript.

References

- Ackerman, W.E., Phero, J.C., Theodore, G.T., 1990. Ineffective ventilation during conscious sedation due to chest wall rigidity after intravenous midazolam and fentanyl. *Anesth. Prog.* 37, 46–8.
- Akata, T., 2007. General anesthetics and vascular smooth muscle: Direct actions of general anesthetics on cellular mechanisms regulating vascular tone. *Anesthesiology*. <https://doi.org/10.1097/00000542-200702000-00026>
- Buchaillard, S., Brix, M., Perrier, P., Payan, Y., 2007. Simulations of the consequences of tongue surgery on tongue mobility: Implications for speech production in post-surgery conditions. *Int. J. Med. Robot. Comput. Assist. Surg.* 3, 252–261. <https://doi.org/10.1002/rcs.142>
- Buchaillard, S., Perrier, P., Payan, Y., 2009. A biomechanical model of cardinal vowel production: muscle activations and the impact of gravity on tongue positioning. *J. Acoust. Soc. Am.* 126, 2033–2051. <https://doi.org/10.1121/1.3204306>
- Budday, S., Sommer, G., Birkl, C., Langkammer, C., Haybaeck, J., Kohnert, J., Bauer, M., Paulsen, F., Steinmann, P., Kuhl, E., Holzapfel, G.A., 2017. Mechanical characterization of human brain tissue. *Acta Biomater.* 48, 319–340. <https://doi.org/10.1016/j.actbio.2016.10.036>
- Buxton, J.A., Gauthier, T., Kinshella, M.-L.W., Godwin, J., 2018. A 52-year-old man with fentanyl-induced muscle rigidity. *CMAJ* 190, E539–E541. <https://doi.org/10.1503/cmaj.171468>
- Cheng, S., Gandevia, S.C., Green, M., Sinkus, R., Bilston, L.E., 2011. Viscoelastic properties of the tongue and soft palate using MR elastography. *J. Biomech.* 44, 450–454. <https://doi.org/10.1016/j.jbiomech.2010.09.027>
- Clayton, E.H., Garbow, J.R., Bayly, P. V, 2011. Frequency-dependent viscoelastic parameters of mouse brain tissue estimated by MR elastography. *Phys. Med. Biol.* 56, 2391–2406. <https://doi.org/10.1088/0031-9155/56/8/005>
- Costa Bandeira, A.K., Azevedo, E.H.M., Vartanian, J.G., Nishimoto, I.N., Kowalski, L.P., Carrara-De Angelis, E., 2008. Quality of life related to swallowing after tongue cancer treatment. *Dysphagia* 23, 183–192. <https://doi.org/10.1007/s00455-007-9124-1>
- Davies, A.E., Stone, S.P., Kidd, D., MacMahon, J., 1995. Pharyngeal sensation and gag reflex in healthy subjects. *Lancet* 345, 487–488. [https://doi.org/10.1016/S0140-6736\(95\)90584-7](https://doi.org/10.1016/S0140-6736(95)90584-7)
- Dimitriou, V., Zogogiannis, I., Liotiri, D., Wambi, F., Tawfeeq, N., Koumi, A., Geldhof, G., 2014. Impossible mask ventilation after an unusually low dose fentanyl-induced muscle rigidity in a patient with essential tremor: A case report and review of the literature. *Middle East J. Anesthesiol.* 22, 619–622.
- Elahi, S.A., Connesson, N., Chagnon, G., Payan, Y., 2019. In-vivo soft tissues mechanical characterization: volume-based respiration method validated on silicones. *Exp. Mech.* 59, 251–261. <https://doi.org/10.1007/s11340-018-00440-9>
- Elahi, S.A., Connesson, N., Payan, Y., 2018. Disposable systems for in-vivo mechanical characterization of soft tissue based on volume measurement. *J. Mech. Med. Biol.* 18. <https://doi.org/10.1142/S0219519418500379>
- Fujita, S., Dang, J., Suzuki, N., Honda, K., 2007. A Computational Tongue Model and its Clinical Application. *Oral Sci. Int.* 4, 97–109. [https://doi.org/10.1016/S1348-8643\(07\)80004-8](https://doi.org/10.1016/S1348-8643(07)80004-8)

- Fung, Y.C.B., 1973. Biorheology of soft tissues. *Biorheology* 10, 139–155. <https://doi.org/10.3233/BIR-1973-10208>
- Gefen, A., Margulies, S.S., 2004. Are in vivo and in situ brain tissues mechanically similar? *J. Biomech.* 37, 1339–1352. <https://doi.org/10.1016/j.jbiomech.2003.12.032>
- Gerard, J.M.M., Ohayon, J., Luboz, V., Perrier, P., Payan, Y., 2005. Non-linear elastic properties of the lingual and facial tissues assessed by indentation technique: Application to the biomechanics of speech production. *Med. Eng. Phys.* 27, 884–892. <https://doi.org/10.1016/j.medengphy.2005.08.001>
- Hermant, N., Perrier, P., Payan, Y., 2017. Human Tongue Biomechanical Modeling, in: Payan, Y., Ohayon, J.B.T.-B. of L.O. (Eds.), *Biomechanics of Living Organs: Hyperelastic Constitutive Laws for Finite Element Modeling*. Academic Press, Oxford, pp. 395–411. <https://doi.org/10.1016/B978-0-12-804009-6.00019-5>
- Horgan, C.O., 2015. The remarkable Gent constitutive model for hyperelastic materials. *Int. J. Non. Linear Mech.* 68, 9–16. <https://doi.org/10.1016/j.ijnonlinmec.2014.05.010>
- Husaini, H., Krisciunas, G.P., Langmore, S., Mojica, J.K., Urken, M.L., Jacobson, A.S., Lazarus, C.L., 2014. A survey of variables used by speech-language pathologists to assess function and predict functional recovery in oral cancer patients. *Dysphagia* 29, 376–386. <https://doi.org/10.1007/s00455-014-9520-2>
- Kappert, K.D.R., van Alphen, M.J.A., Smeele, L.E., Balm, A.J.M., van der Heijden, F., 2019a. Quantification of tongue mobility impairment using optical tracking in patients after receiving primary surgery or chemoradiation. *PLoS One* 14, e0221593. <https://doi.org/10.1371/journal.pone.0221593>
- Kappert, K.D.R., van Alphen, M.J.A., van Dijk, S., Smeele, L.E., Balm, A.J.M., van der Heijden, F., 2019b. An interactive surgical simulation tool to assess the consequences of a partial glossectomy on a biomechanical model of the tongue. *Comput. Methods Biomech. Biomed. Engin.* 22, 827–839. <https://doi.org/10.1080/10255842.2019.1599362>
- Kerdok, A.E., Ottensmeyer, M.P., Howe, R.D., 2006. Effects of perfusion on the viscoelastic characteristics of liver. *J. Biomech.* 39, 2221–2231. <https://doi.org/10.1016/j.jbiomech.2005.07.005>
- Kreeft, A.M., Van Der Molen, L., Hilgers, F.J., Balm, A.J., 2009. Speech and swallowing after surgical treatment of advanced oral and oropharyngeal carcinoma: A systematic review of the literature. *Eur. Arch. Oto-Rhino-Laryngology* 266, 1687–1698. <https://doi.org/10.1007/s00405-009-1089-2>
- Lang, Y.D., Malacina, A., Biegler, L.T., Munteanu, S., Madsen, J.I., Zitney, S.E., 2009. Reduced order model based on principal component analysis for process simulation and optimization, in: *Energy and Fuels*. pp. 1695–1706. <https://doi.org/10.1021/ef800984v>
- Lee, D.Y., Ryu, Y.J., Hah, J.H., Kwon, T.K., Sung, M.W., Kim, K.H., 2014. Long-term subjective tongue function after partial glossectomy. *J. Oral Rehabil.* 41, 754–758. <https://doi.org/10.1111/joor.12193>
- Mann, H.B., Whitney, D.R., 1947. On a Test of Whether one of Two Random Variables is Stochastically Larger than the Other. *Ann. Math. Stat.* 18, 50–60. <https://doi.org/10.1214/aoms/1177730491>
- Mehrabian, H., Samani, A., 2008. An iterative hyperelastic parameters reconstruction for breast cancer assessment, in: *Medical Imaging 2008: Physiology, Function, and Structure from Medical Images*. <https://doi.org/10.1117/12.770971>

- Montero, P.H., Patel, S.G., 2015. Cancer of the oral cavity. *Surg. Oncol. Clin. N. Am.* 24, 491–508. <https://doi.org/10.1016/j.soc.2015.03.006>
- Müller, P., Vogtmann, C., 2000. Three cases with different presentation of fentanyl-induced muscle rigidity - A rare problem in intensive care of neonates. *Am. J. Perinatol.* 17, 23–26. <https://doi.org/10.1055/s-2000-7289>
- Nakada, J., Nishira, M., Hosoda, R., Funaki, K., Takahashi, S., Matsura, T., Inagaki, Y., 2009. Priming with rocuronium or vecuronium prevents remifentanil-mediated muscle rigidity and difficult ventilation. *J. Anesth.* 23, 323–328. <https://doi.org/10.1007/s00540-009-0769-9>
- Nava, A., Mazza, E., Furrer, M., Villiger, P., Reinhart, W.H., 2008. In vivo mechanical characterization of human liver. *Med. Image Anal.* 12, 203–216. <https://doi.org/10.1016/j.media.2007.10.001>
- Ogden, R., 1984. Non-linear elastic deformations. *Eng. Anal. Bound. Elem.* 1, 119. [https://doi.org/10.1016/0955-7997\(84\)90049-3](https://doi.org/10.1016/0955-7997(84)90049-3)
- Pelteret, J.P.V., Reddy, B.D., 2012. Computational model of soft tissues in the human upper airway. *Int. J. Numer. Method. Biomed. Eng.* 28, 111–132. <https://doi.org/10.1002/cnm.1487>
- Rashid, B., Destrade, M., Gilchrist, M.D., 2012. Mechanical characterization of brain tissue in compression at dynamic strain rates. *J. Mech. Behav. Biomed. Mater.* 10, 23–38. <https://doi.org/10.1016/j.jmbbm.2012.01.022>
- Sadeghnejad, S., Elyasi, N., Farahmand, F., Vossughi, G.R., Sadr Hosseini, S.M., 2019. Hyperelastic modeling of sino-nasal tissue for haptic neurosurgery simulation. *Sci. Iran.* 27, 1266–1276. <https://doi.org/10.24200/sci.2019.50348.1652>
- Schiavone, P., Boudou, T., Promayon, E., Perrier, P., Payan, Y., 2008. A light sterilizable pipette device for the in vivo estimation of human soft tissues constitutive laws, in: 2008 30th Annual International Conference of the IEEE Engineering in Medicine and Biology Society. IEEE, pp. 4298–4301. <https://doi.org/10.1109/IEMBS.2008.4650160>
- Schiavone, P., Chassat, F., Boudou, T., Promayon, E., Valdivia, F., Payan, Y., 2009. In vivo measurement of human brain elasticity using a light aspiration device. *Med. Image Anal.* 13, 673–678. <https://doi.org/10.1016/j.media.2009.04.001>
- Schiavone, P., Promayon, E., Payan, Y., 2010. LASTIC: A Light Aspiration Device for in vivo Soft Tissue Characterization, in: *Lecture Notes in Computer Science (Including Subseries Lecture Notes in Artificial Intelligence and Lecture Notes in Bioinformatics)*. pp. 1–10. https://doi.org/10.1007/978-3-642-11615-5_1
- Schwarte, L., Loer, S., Schober, P., 2008. Effects of thiopental and propofol on skeletal muscle oxygenation. *Eur. J. Anaesthesiol.* 25, 60. <https://doi.org/10.1097/00003643-200805001-00186>
- Sessions, D.G., Spector, G.J., Lenox, J., Haughey, B., Chao, C., Marks, J., 2002. Analysis of treatment results for oral tongue cancer. *Laryngoscope* 112, 616–25. <https://doi.org/10.1097/00005537-200204000-00005>
- Shah, J.P., Gil, Z., 2009. Current concepts in management of oral cancer – Surgery. *Oral Oncol.* 45, 394–401. <https://doi.org/10.1016/j.oraloncology.2008.05.017>
- Stavness, I., Lloyd, J.E., Fels, S., 2012. Automatic prediction of tongue muscle activations using a finite element model. *J. Biomech.* 45, 2841–2848. <https://doi.org/10.1016/j.jbiomech.2012.08.031>

- Tagaito, Y., Isono, S., Nishino, T., 1998. Upper airway reflexes during a combination of propofol and fentanyl anesthesia. *Anesthesiology* 88, 1459–1466. <https://doi.org/10.1097/00000542-199806000-00007>
- Van Alphen, M.J.A., Kreeft, A.M., Van Der Heijden, F., Smeele, L.E., Balm, A.J.M., 2013. Towards virtual surgery in oral cancer to predict postoperative oral functions preoperatively. *Br. J. Oral Maxillofac. Surg.* 51, 747–751. <https://doi.org/10.1016/j.bjoms.2013.06.012>
- van der Molen, L., van Rossum, M.A., Jacobi, I., Van Son, R.J.J.H.J.H., Smeele, L.E., Rasch, C.R.N.N., Hilgers, F.J.M.M., 2012. Pre- and posttreatment voice and speech outcomes in patients with advanced head and neck cancer treated with chemoradiotherapy: Expert listeners' and patient's perception. *J. Voice* 26, 664.e25-664.e33. <https://doi.org/10.1016/j.jvoice.2011.08.016>
- Vogt, F., Lloyd, J., Buchaillard, S., Perrier, P., Chabanas, M., Payan, Y., Fels, S., 2006. Efficient 3d finite element modeling of a muscle-activated tongue. *Lect. Notes Comput. Sci.* 19–28.
- Wang, Y.K., Nash, M.P., Pullan, A.J., Kieser, J.A., Rohrle, O., 2013. Model-based identification of motion sensor placement for tracking retraction and elongation of the tongue. *Biomech. Model. Mechanobiol.* 12, 383–399. <https://doi.org/10.1007/s10237-012-0407-6>
- Wilcoxon, F., 1947. Probability Tables for Individual Comparisons by Ranking Methods. *Biometrics* 3, 119. <https://doi.org/10.2307/3001946>
- Wilhelms-Tricarico, R., 1995. Physiological modeling of speech production: methods for modeling soft-tissue articulators. *J. Acoust. Soc. Am.* 97, 3085–3098. <https://doi.org/10.1121/1.411871>
- Yeoh, O.H., 1993. Some forms of the strain energy function for rubber. *Rubber Chem. Technol.* 66, 754–771. <https://doi.org/10.5254/1.3538343>